Pharm Res (2010) 27:933–942
DOI 10.1007/s11095-010-0100-3

RESEARCH PAPER

Folate-PEG-CKK$_2$-DTPA, A Potential Carrier for Lymph-Metastasized Tumor Targeting

Bing Gu • Cao Xie • Jianhua Zhu • Wei He • Weiyue Lu

Received: 15 October 2009 / Accepted: 22 February 2010 / Published online: 11 March 2010

ABSTRACT

Purpose A novel conjugate, Folate-PEG-CKK$_2$-DTPA, was designed and prepared as a carrier for lymphatic metastasized tumor imaging diagnosis and targeting therapy.

Methods Folate-PEG-CKK$_2$-DTPA was synthesized and characterized by analysis High Performance Liquid Chromatography, Size Exclusive Chromatography and ^{1}H-NMR. ^{99m}Tc-labeled conjugation was prepared, and *in vivo* quantitative biodistribution and SPECT imaging were studied after subcutaneously injected into the rats and rabbits, respectively. Cell uptake study was carried in a KB cell line using fluorescent methods. *In vivo* and *ex vivo* fluorescent imaging study was carried in tumor-bearing nude mouse to evaluate its targeting ability.

Results Folate-PEG-CKK$_2$-DTPA was synthesized with high purity. Both *in vivo* biodistribution study and SPECT imaging study show the rapid direction and high distribution of the conjugation to the lymph nodes. The uptake of fluorescence-labeled Folate-PEG-CKK$_2$-DTPA in human oral epidermis carcinoma cells was observed. *In vivo* and *ex vivo* fluorescent imaging study indicated it could accumulate in tumor region after vein tail injection in nude mouse.

Conclusions All these findings suggested Folate-PEG-CKK$_2$-DTPA as a novel and dependable carrier for tumor diagnosis and therapy, especially for lymph-metastasized tumors.

KEY WORDS fluorescent imaging · folate-PEG-CKK$_2$-DTPA · lymph targeting · radio active tracing · tumor targeting

B. Gu • C. Xie • J. Zhu • W. Lu (✉)
School of Pharmacy, Fudan University,
826 Zhangheng Road,
Shanghai 201203, China
e-mail: wylu@shmu.edu.cn

W. He
Department of Nuclear Medicine, Huadong Hospital,
Shanghai 200040, China

ABBREVIATIONS

BCS	Bull Calf Serum
CKK$_2$	cysteine-L-lysine-(L-lysine)$_2$
DIPEA	N,N-Diisopropylethylamine
DMSO	dimethyl sulfoxide
DTPA	diethylenetriaminepentaacetic acid
EDA	Ethylenediamine
EDC·HCl	1-Ethyl-3-(3-dimethyllaminopropyl) carbodiimide hydrochloride
FBS	Fetal bovine serum
FITC	Fluorescein-5-isothiocyanate
FR	Folate receptor
HBTU	O-Benzotriazole-N,N,N′,N′-tetramethyl-uronium-hexafluorophosphate
HF	hydrogen fluoride
HOBT	Hydroxybenzotriazole
HPLC	high-performance liquid chromatography
KB	human oral epidermoid carcinoma
Mal-PEG-NHS	maleimide-polyethyl glycol-succinimidyl ester
ROI	Region of Interest
SPECT	Single-Photon-Emission Computed Tomography
TFA	trifluoacetic acid
^{1}H NMR	^{1}H nuclear magnetic resonance

INTRODUCTION

Early diagnosis of metastasized tumors in cancer patients, especially in patients with epithelial origin cancer like breast, colon, lung, ovary, and prostate cancer, has come to the forefront as a global challenge in cancer therapy (1,2). Accurate staging of lymph nodes is a critical component in determining the possibility of metastasis, which dictates the therapeutic options. Although sentinel node biopsy has been

an improvement over histological microscopy, its invasive nature brings sufferings and inconvenience to patients. Many noninvasive methods have been employed for lymph metastasized tumor diagnosis, including cross-sectional imaging using radiolabeled colloid nanoparticles, single hybrid probe for Magnetic Resonance, Near Infrared optical imaging and the combinational technology (3–7). However, all the techniques described above have low specificity for malignant lymph nodes (8) and high false-positive probability in diagnosis (9). In the meantime, treatment of lymph metastasized tumors is of the same great significance and difficulty. Available methods, including liposomes carrying antineoplastic agents, intralymphatic chemotherapy using a Hyaluronan-Cisplatin conjugate and adenovirus gene transfer vectors for inhibition of lymph metastasis (10–14), are not satisfactory because of the prolonged local tissue damage caused by drug leakage from drug delivery systems after subcutaneous injection (15). Consequently, the high incidence of metastasis and the limited advances in lymphatic diagnostic or therapeutic delivery systems necessitates the development of a novel vector system specifically targeted to malignant lymph nodes.

To confer delivery systems, targeting capability to malignant lymph nodes, we cannot emphasize enough the importance of selecting a suitable targeting ligand. Folic acid is the most versatile small molecule for tumor targeting. Folate receptor is over-expressed on a variety of human cancers, including cancers of the breast, ovaries, endometrium, lungs, kidneys, colon, brain, and myeloid cells of hematopoietic origin (16). Most importantly, expression of FR positivity seems more frequent in metastasized carcinoma than primaries (44% compared to 33%) in colorectal carcinoma (17). For example, folate receptor was found to be expressed in a significant proportion of both primary squamous cell carcinoma of the head and neck and corresponding lymph node metastases tissues, and the expression level correlated well with clinical outcome (18). As a natural vitamin, folate acid showed high affinity to folate receptor, providing us a targeting strategy to develop biomaterials for the delivery of imaging agents or chemotherapy agents to FR-positive tumors, including malignant lymph nodes. Previous reports confirmed the use of folate receptor-mediated optical imaging for visualizing metastatic tumor loci of sub-millimeter size (19). The safety and feasibility of Folate-DTPA-^{111}In and ^{99m}Tc-EC20 (^{99m}Tc-pteroic acid-d-Glutamine-β-l-diaminopropionic acid-Aspartic acid-Cystine, a folate containing peptide) for scintigraphy differentiating between malignant and benign tissues has been proven in a series of clinical research (20–22). However, FR-mediated drug delivery system for lymph-metastasized tumor targeting has been rarely addressed for so far.

The agent for lymph-metastasized tumor imaging or treatment should be capable of differentiating between enlarged hyperplastic lymph nodes and metastatic nodes. Fast clearance from the normal lymph system is critical for precise diagnosis and reduced retention of chemotherapeutic agents in local lymphatic tissues. With this in mind, PEGylation has been suggested as an effective approach since the inclusion of PEG in lymph target delivery systems helped the drainage of liposomes to non-macrophage targets and increase the distribution of the liposomes in the normal lymph nodes (23,24).

DTPAs are widely used to chelate radionuclide for radio imaging and therapy, especially for ^{99m}Tc- and ^{111}In-based radiopharmaceutical (25). The multiple terminal carboxy groups of DTPA facilitate carrying more imaging agents and therapeutic agents. With more nuclide chelated, DTPA can give images with high spatial resolution in diagnosis of micro-metastasis in lymphatic system. The affluent carboxy groups of terminal DTPA could potentially provide a convenient graft for chemotherapy agents like doxorubicin, cis-platinum, paclitaxel, *et al.*

Herein, we designed and prepared a novel bioconjugate composed of folate, PEG and *p*-SCN-Bn-DTPA as an imaging vector targeted to malignant lymph nodes for the early diagnosis of metastasis. A peptide composed of four terminal amino groups was included in the conjugate to carry more DTPA. *In vivo* biodistribution in rats of this ^{99m}Tc-labeled conjugate was evaluated after subcutaneous injection into the footpad. The imaging effect of the ^{99m}Tc-labeled conjugate was studied by SPECT imaging and ROI analysis in rabbits. The tumor targeting ability of the FITC-labeled conjugate was investigated by the endocytosis study in KB cells *in vitro* and in tumor-bearing nude mice *in vivo*, respectively.

MATERIALS AND METHODS

Materials

Folic acid-polysaccharide complex was self-made with ester linkage. Mal-PEG-NHS, MW 2000, was purchased from JenKem Techno- logical Ltd. Co. of Beijing, China. Boc-Cys (Mbzl)-PAM resin, FITC and EDA were obtained from Sigma-Aldrich (St. Louis, MO, USA). EDC·HCl, Boc-Lysine (Boc) and HOBT were purchased from Gil Bio (Shanghai, China). *p*-SCN-Bn-DTPA was purchased from Macrocyclics (Dallas, TX, USA). HBTU was purchased from American Bioanalytical (Natick, MA, USA). $Na^{99m}TcO_4$ was gifted from Department of Radiology, Zhongshan Hospital (Shanghai, China). FBS, RPMI 1640 medium and folate-free RPMI 1640 medium were purchased from Gibco Co., USA. Acetonitrile, methanol and other HPLC grade reagents were obtained from Fisher Scientific, USA. Anhydrous diethyl ether, sodium chloride, DMSO and other

chemicals reagents methanol used were obtained from Sinopharm Chemical Reagent Co., Ltd., China.

Preparation of Folate-PEG-CKK$_2$-DTPA

Synthesis of Folate-EDA

Ten mg of Folic acid-polysaccharide complex was gradually added into 66 mL of EDA and stirred at room temperature in the dark for 3 h. The reaction solution was added into 750 mL acetone to obtain the precipitation. After it was washed with 250 mL acetone twice, the precipitation was dissolved in water and filtrated to remove the insoluble substance. Folate-EDA was obtained as dark red solid when the pH of the solution was adjusted to 7.0 using chlorhydric acid (1 M). The product was freeze-dried after washing with water and acetone in turns three times. The analytical HPLC was conducted on an Agilent 1100 series quaternary HPLC system (Palo Alto, CA, USA) equipped with a vacuum degasser, an autosampler, a thermostetted column, and a UV and refractive index detector. The chemical purity of Folate-EDA was examined by analytical HPLC on a Diamonsil C18 Column (5 μm particle size, 200×4.6 mm, Dikma Technologies) at 40°C (eluant A, water with 0.1% TFA; eluant B, acetonitrile with 0.1% TFA; gradient, 5–65% B over 30 min at a flow rate of 0.7 mL/min).

Synthesis of Folate-PEG-Mal

Twelve mg (0.024 mmol) of Folate-EDA was dispersed in 2.5 mL DMSO and sonicated for 30 min until dissolved. Mal-PEG-NHS (32 mg, 0.016 mmol) was slowly added. The mixture was stirred for 30 min in the dark at 25°C. The Folate-PEG-Mal was then separated from Folate-EDA and DMSO using a Sephadex G-15 gel column (15 mm× 30 cm) on a ÄKTA explorer 100 system (Amersham Biosciences, Uppsala, Sweden) consisting of Pump P-900, Pump P-950, Monitor UV-900, and Frac-900 at room temperature. The column was washed with deionized water at a flow rate of 1 mL/min. Fractions were collected and lyophilized.

Analytical chromatography was performed on an Agilent 1100 series quaternary HPLC system same as described in *Synthesis of Folate-EDA*. The chemical purity of Folate-PEG-Mal was examined on a YMC-ODS column (5 μm particle size, 300Å pore size, 150×4.6 mm) at 40°C using a linear gradient same as described as 2.2.1. ^{1}H NMR (500 MHz, D_2O) δ(ppm) for Folate-PEG-Mal: ~8.5–8.6 (s, C7-H, 1H), ~7.4–7.5 (d, 2′,6′-H, 2H), ~6.6–7.7 (d, 3′,5′-H, 2H), ~4.2–4.3 (minor and major α-CH2 of Glu, 1H), and ~2.0–2.4 (m, β, γ-CH_2 of GLu, 4H) for folate; ~3.1–4.0 (m, -OCH2CH2) and 6.94 (d, 2′,3′-H, 2H of Maleimide) for Mal-PEG-NHS.

Synthesis of CKK$_2$

CKK$_2$ was synthesized using a Boc-protected solid phase peptide synthesis procedure. Generally, Boc-Cys(pMeBzl)-PAM resin was pre-swollen in DMF, deprotected using TFA and washed with DMF. The coupling procedure was performed using 3 eq. of HBTU, 8.8 eq. Boc-Lys(Boc)-OH acid and 6 eq. of DIPEA calculated according to the substitution level of the resin. After 30 min of the coupling for one step, the resin was washed with DMF, deprotected with TFA and coupled with Boc-Lys(Boc)-OH in another cycle as described.

Final cleavage of the peptidyl resin and side chain deprotection was conducted using HF at 4°C for 2 h. Then the product was precipitated and washed with anhydrous diethyl ether and freeze-dried. Analytical HPLC was performed using the same system and C18 column as described in *Synthesis of Folate-EDA* at 40°C (eluant A, water with 0.1% TFA; eluant B, acetonitrile with 0.1% TFA; gradient, 0 to 10% B over 30 min at a flow rate of 0.7 mL/min). The retention time of the product was 19.4 min. High resolution mass spectroscopy (Agilent, CA, USA): CKK$_2$, $[M+H]^+$ 506.30, found 506.45.

Synthesis of Folate-PEG-CKK$_2$

Ten mg (0.004 mmol) of Folate-PEG-Mal was dissolved in 500 μL phosphate buffer (10 mmol/L, pH 7.4). Five mg (0.01 mmol) CKK$_2$ was added into the solution and stirred for 30 min in the dark at a nitrogen atmosphere. After filtrated with a 0.45 μm film, the mixture was desalted using a Sephadex G-15 gel column (15 mm×30 cm) on an ÄKTA explorer 100 systems. Fractions were collected and lyophilized. HPLC was performed to examine the purity of the product using the same system and method described in *Synthesis of CKK$_2$*. ^{1}H NMR (500 MHz, D_2O) δ(ppm) for Folate-PEG-CKK$_2$: ~8.5–8.6 (s, C7-H, 1H), ~7.4–7.5 (d, 2′,6′-H, 2H), ~6.6–7.7 (d, 3′,5′-H, 2H), ~4.2–4.3 (minor and major α-CH2 of Glu, 1H), and ~2.0–2.4 (m, β, γ-CH_2 of GLu, 4H) for folate; 4.78 (s, α-H of Cys, 1H), 4.42 (s, α-H of Lys, 1H) for CKK$_2$, and ~3.1–4.0 (m, -OCH_2CH_2) for NHS-PEG-Mal.

Synthesis of Folate-PEG-CKK$_2$-DTPA

Six mg (0.002 mmol) Folate-PEG-CKK$_2$ was dissolved in 500 μL DMF. Six mg of p-SCN-Bn-DTPA was added into

the solution and stirred in the dark for 3 h. Kaiser Test (26) was conducted to confirm the reaction of terminal amino groups. DMF and excess p-SCN-Bn-DTPA was removed using a Sephadex G-15 gel column (15 mm × 30 cm) on an ÄKTA explorer 100 systems at a flow rate of 1 ml/min (eluant: 0.1 M HAc-NaAc solution with 20% EtOH, pH 3.2). Fractions were collected and lyophilized. Analytical HPLC was performed to examine the purity of the product on a TSK-GEL G4000PWXL colum (10 μm particle size, 300Å pore size, Tosoh Corporation, Minato-ku, Tokyo, Japan) using the HPLC system described before at a flow rate of 0.5 mL/min with deionized water as the eluent. 1H NMR (500 MHz, D_2O) δ(ppm) for Folate-PEG-CKK_2-DTPA: ~8.5–8.6 (s, C7-H, 1H), ~7.5–8.0 (d, 2′,6′-H, 2H), ~6.6–7.7 (d, 3′,5′-H, 2H), ~4.2–4.3 (minor and major α-CH2 of Glu, 1H), and ~2.0–2.4 (m, β, γ-CH_2 of GLu, 4H) for folate; ~3.1–4.0 (m, -OCH2CH2) for Mal-PEG-NHS,4.78 (s, α-H of Cys, 1H), 4.42 (s, α-H of Lys, 1H) for CKK_2 and ~7.0–7.5 (d, 2′,3′,5′,6′-H) for *p*-SCN-Bn-DTPA.

In Vivo Study of Folate-PEG-CKK_2-DTPA

^{99m}Tc Labeling of Folate-PEG-CKK_2-DTPA

Folate-PEG-CKK_2-DTPA was labeled with ^{99m}Tc using the Tin(II) Chloride Reduction method as described previously (27). Briefly, 208 μL of Folate-PEG-CKK_2-DTPA (25 mg/mL) in 10 mmol/L phosphate buffer (pH 7.2, 0.9%NaCl) was mixed with 35 μL solution of tin chloride (10 mg $SnCl_2{\cdot}2H_2O$ in 10 mL of 0.1 mol/L HCl). The mixture was diluted with phosphate buffer to 0.5 mL and then incubated with freshly eluted 0.5 mL (740 MBq/mL) of $Na^{99m}TcO_4$ for 15 min at room temperature. The radiochemical purity of radiolabeled compound was analyzed by paper chromatography to determine the unbound $Na^{99m}TcO_4$ and the [^{99m}Tc] colloid (28).

Biodistribution in Rats

The biodistribution of the conjugate was investigated after injection of ^{99m}Tc-labeled Folate-PEG-CKK_2-DTPA into footpad of Wistar rats (male, 3 weeks). Each rat was injected with ^{99m}Tc-labeled conjugate (50 μL, 370 MBq/ml) into the footpad of right side. Three rats were sacrificed for each time point after 10 min, 30 min, 1 h, 2 h and 4 h, respectively. Popliteal, iliac and inguinal lymph nodes of right sides and other major tissues were excised and assayed for radioactivity. The biodistribution of the tracer in each animal was calculated as a percentage of injected dose per gram of tissue wet weight (%ID/g), using reference counts from an accurately diluted sample of the original injection.

Imaging in Rabbit

Folate-PEG-CKK_2-DTPA-^{99m}Tc (50 μL, 5 mg/mL, 18.5 MBq) was injected into the web space between the second and third digiti pedis in both hind limbs of a normal rabbit. Then the sequential 5-min SPECT scans were performed in whole body to get the radio images (Siemens ECAM dual-head) at 5, 15, 30, 60, 120, 180, 240, 300, 360 min. The scintigraphic images were analyzed by drawing the ROI on the lymph nodes and calculating the radiocounting of ROI according to the decay property of ^{99m}Tc.

Tumor Uptake Studies

Fluorescent Labeling of Folate-PEG-CKK_2-DTPA

The synthesis of EDA-FITC and labeling of Folate-PEG-CKK_2-DTPA were as previously described (27). Briefly, FITC was reacted with 50 mol eq. of EDA. Preparative HPLC was conducted to purify EDA-FITC, which reacted with Folate-PEG-CKK_2-DTPA in a DMF solution with HOBt (1.2 eq.) and EDA (1.2 eq.) in dark for 3 h at room temperature. The fluorescent-labeled conjugation was purified using a Sephadex G-15 gel column (15 mm × 30 cm) in an ÄKTA explorer system described in the section before.

Tumor Cell Uptake Test

KB Cells (purchased from ATCC, cultured in RPMI1640 cell culture medium with 10% heat-inactivated BCS at 37° C, 5% CO_2) plated at 1×10^5 cells per well density in 24-well plates were first cultured with folate-free RPMI 1640 medium overnight with 10% (v/v) heating-activated FBS. Then the cells were incubated with 2×10^{-7}M solution of FITC-labeled Folate-PEG-CKK_2-DTPA for 3 h at 37°C. For folate competition groups, 1 mM folic acid was added in the culture medium. The cell uptake was determined by FITC fluorescence on an Olympus Image-Pro Plus fluorescence microscope (Japan).

Tumor Tissue Uptake Test

In vivo and *ex vivo* fluorescent imaging was carried in KB tumor-bearing nude mice using a NightOWL II LB 983 imaging system (Berthold Technologies, Germany). To capture fluorescent imaging, the mouse was then anesthetized with 10% chloraldurat 2 h after vein tail injection of 1 mg/100 μL Folate-PEG-CKK_2-DTPA labeled with FITC. After taking images *in vivo*, the mice were sacrificed to excise major organs which were photographed *ex vivo*.

RESULTS

Preparation and Characterization of Folate-PEG-CKK$_2$-DTPA

As shown in Fig. 1., the synthesis pathway was composed of four steps. Folate-EDA was prepared with folic acid-polysaccharide complex and excess neat ethylenediamine, obtaining a mixtured product containing 86.22% Folate (γ)-EDA (retention time 14.0) and 9.06% Folate(α)-EDA (retention time 14.9). Then Folate-EDA was conjugated to bifunctional PEG through the active NHS group. Due to the high reaction activity of NHS, this reaction could be finished in 30 min at room temperature. The only impurity in this step was superfluous Folate-EDA which could be purified by precipitation with water and gel chromatography. Using the Boc protected solid phase peptide synthesis technique, the cysteine-terminated poly(L-lysine) (CKK$_2$) was synthesized with high purity through precipitation and washing with diethyl ether after cleavage from the resin. HPLC results of Folate-PEG-Mal and Folate-PEG-CKK$_2$ (Fig. 2) showed the high purity of these intermediate products (>95%).

We chose bifunctional conjugate *p*-SCN-Bn-DTPA instead of DTPA dianhydrate to simplify the synthesis and purification procedure, because both of the two anhydride groups in DTPA dianhydrate were very likely to react with the terminal amino-groups of CKK$_2$ without selectivity, leaving less free carboxy groups for chelating radio nuclides. The HPLC result (Fig. 3) indicated a purity higher than 95% for the target product Folate-PEG-CKK$_2$-DTPA, and 1-H NMR data (Fig. 3) suggested the number of *p*-SCN-Bn-DTPA per molecular to be about 3.9 according to the ratio of C7-H to C-2′,3′,5′,6′-H.

Lymphatic System Targeting of Folate-PEG-CKK$_2$-DTPA

Before starting *in vivo* biodistribution study with ^{99m}Tc-labeled Folate-PEG-CKK$_2$-DTPA, the radiochemical purity of the radiolabeled conjugation was first determined by paper chromatography to be higher than 95%, and the impurities were mostly in the form of colloid ^{99m}Tc.

Lymphatic System Targeting Distribution in Rats

Fig. 4 shows the %ID/g radiocounting for the popliteal, iliac, inguinal lymph nodes and other tissues at 15 and 30 min, 1, 2 and 4 h post-administration of Folate-PEG-CKK$_2$-DTPA-^{99m}Tc in rats. The amount of radioactivity in popliteal nodes was 4.82 %ID/g at 10 min, increased to the maximum of 5.78 %ID/g and then decreased to 1.58 %ID/g at 4 h. The maximum amount in popliteal nodes was about 85 times as in the blood (0.068%ID/g) and 35 times as in the kidney (0.78%ID/g), respectively. The distribution of the conjugate in other organs was even less than that in the kidney. The fast accumulation and clearance of Folate-PEG-CKK$_2$-DTPA in normal lymph nodes observed here were beneficial to target malignancy of lymph nodes.

Lymphatic System Imaging and Pharmacokinetics in Rabbits

Fig. 5A shows the imaging results in rabbits 3 h after injection of Folate-PEG-CKK$_2$-DTPA-^{99m}Tc. At least 3 lymph nodes could be imaged in one hind limb of rabbits. The lymphatic vessels, popliteal and inguinal lymph nodes showed prominent signals 5 min after injection and faded for the following hours while the signal from other lymph nodes in the hind limb became increasingly stronger at the same time and then faded as time later elapsed. The radio activity ROI on the popliteal lymph node of right hind limb indicated a fast clearance in popliteal lymph nodes for 1 h and maintenance at a low level for the sequential 5 h (Fig. 5B).

Tumor Target of Folate-PEG-CKK$_2$-DTPA

As shown in Fig. 6, the fluorescent-labeled conjugate could be taken up by KB cells and blocked by the competition of free folic acid, indicating a possible endocytosis mechanism mediated by folate receptor. Fluorescent imaging *in vivo* and *ex vivo* indicated an accumulation of the conjugate in a transplanted KB tumor in mice (Fig. 7), in agreement with results from the *in vitro* endocytosis study. A high level of fluorescent signal was also observed in kidneys.

DISCUSSIONS

Cancer of epithelial origin, including breast, colon, lung, ovary, and prostate cancer, holds high risk to spread through lymph vessels (2). Nowadays, to monitor and preclude metastasis, sentinel lymph node (SLN) mapping is widely used in patients with epithelia tumor even without any clinical evidence of nodal metastases, because early lymphatic metastases, if present, always occur within the SLN, the first tumor-draining lymph node. Therefore, accurate and sensitive imaging of lymph-metastasized tumor is of significance for the early diagnosis and therapy for malignant cancer. Besides the sentinel lymph nodes, detection of other malignant lymph nodes in lymphatic system could also provide valuable information for early tumor staging, guidance for excision of the tumor and follow-up for recovery after surgery.

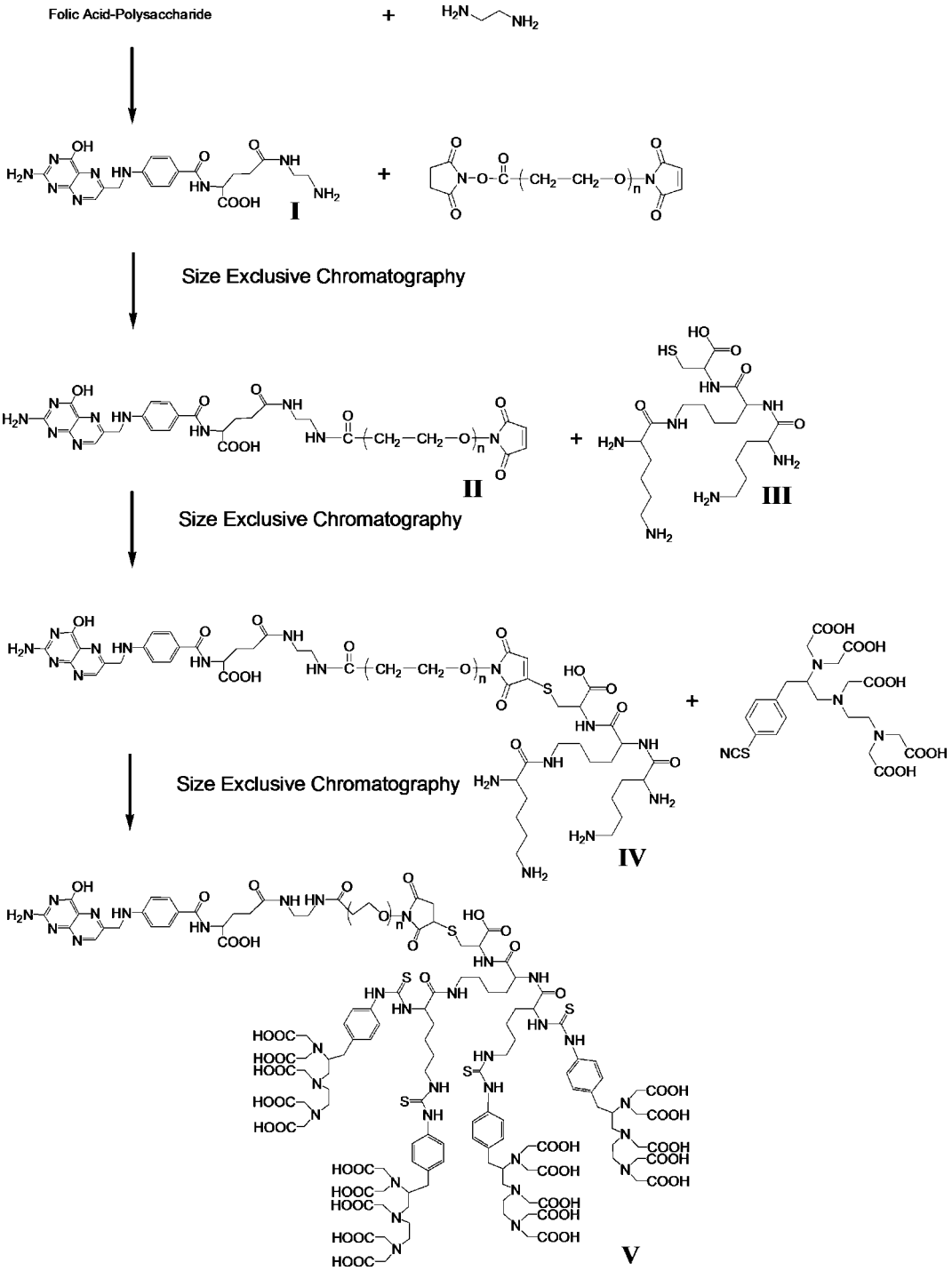

Fig. 1 Synthesis Scheme of Folate-PEG-CKK_2-DTPA, the number of the chemical structures represents the chemical names as follows: I for Folate-EDA, II for Folate-PEG-Mal, III for CKK_2, IV for Folate-PEG-CKK_2, IV for Folate-PEG-CKK_2 and V for Folate-PEG-CKK_2-DTPA.

To realize active tumor targeting, folic acid was used to modify DTPA-based nuclide vector. According to previous literature (29–31), both α- and γ- derivatives of folate possessed similar high affinity to folate receptor, so the obtained compound of Folate-EDA (including both α- and γ-derivatives) was directly used for follow-up synthesis without separation. The polyethylene glycol, serving as a hydrophilic backbone, could effectively evade the recognition and phagocytosis by macrophage cells in lymphatic system and avoid possible fast clearance of Folate-PEG-CKK_2-DTPA in the lymph system. A multi-lysine terminated peptide (CKK_2) was included in the conjugate in order to carry more DTPA and thus chelate more nuclide imaging agents or conjugate more chemotherapeutic agents. The four terminal amino groups

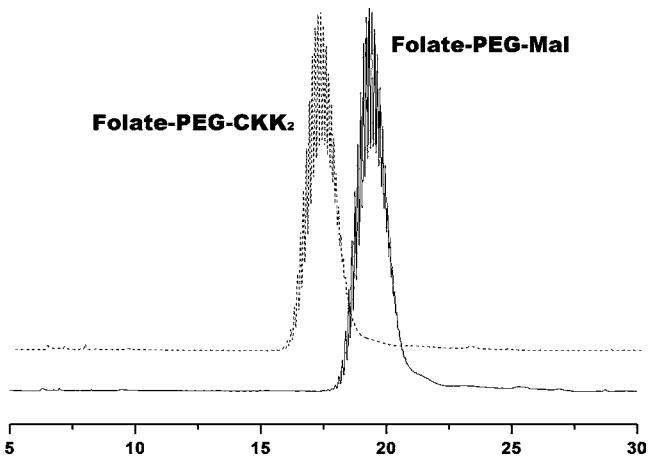

Fig. 2 HPLC results of Folate-PEG-CKK_2 and Folate-PEG-Mal. HPLC was performed on a YMC C18 Column (5 μm particle size, 300Å pore size, 150 × 4.6 mm) at 40°C (eluant A, water with 0.1% TFA; eluant B, acetonitrile with 0.1% TFA; gradient, 5–65% B over 30 min at a flow rate of 0.7 mL/min; detection UV @280 nm).

could conjugate a maximum of four chelating agents, which could increase the resolution of the imaging agents and therapeutic effects of chemotherapeutics, providing a good solution for early diagnosis of metastasized tumor with small size and target therapy for lymphatic malignancies.

Traditionally, DTPA dianhydride was used for reaction. The less selectivity of the reaction with bisanhydride may also lead to the yield of conjugates containing the ligand weaker than DTPA (32). Therefore, monofunctional DTPA (*p*-SCN-Bn-DTPA) was preferred for the prepara-

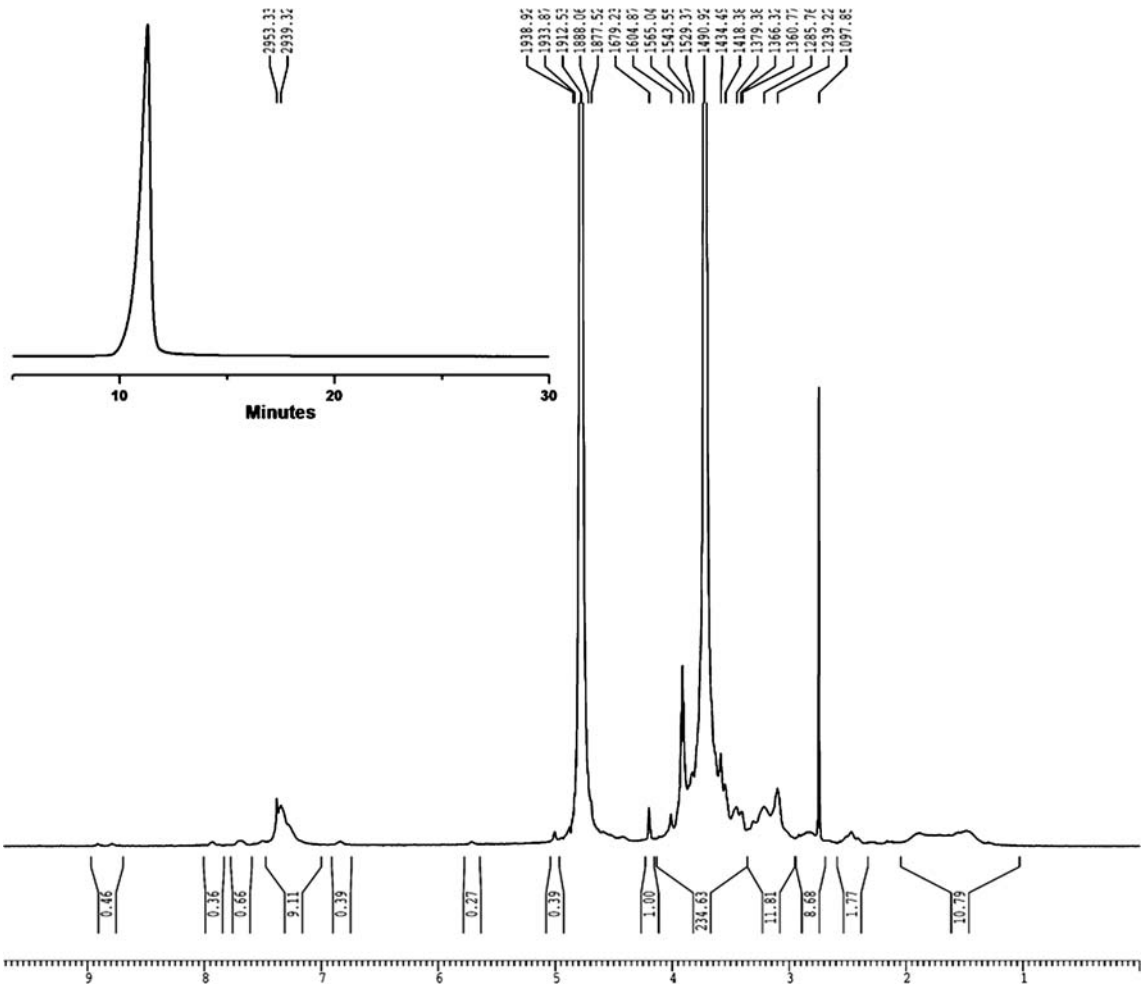

Fig. 3 HPLC result and 1-H NMR result of Folate-PEG-CKK_2-DTPA. HPLC was carried on a TSK-GEL G4000PWXL column at a flow rate of 0.5 mL/min with deionized water as eluent, detection UV@280 nm.

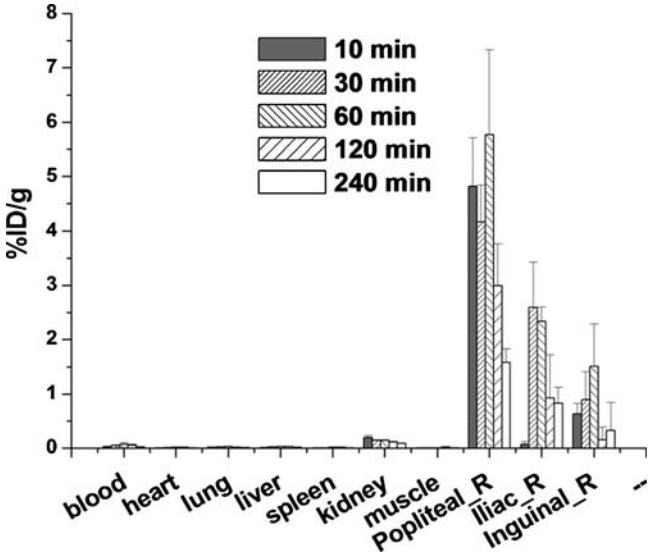

Fig. 4 *In vivo* biodistribution of Folate-PEG-CKK_2-DTPA-^{99m}Tc after injection in footpad of rats at different time points. All data are expressed as mean ± standard deviation ($n = 3$).

tion of DTPA conjugation to obtain products with high stability and selectivity.

Subcutaneous (SC) injections has been considered preferable for delivery in the lymphatic system, as the absorption of small particulates and macromolecules into blood are restricted by the vascular endothelia (33) and can be drained to the lymphatic capillaries and subsequently transported to regional lymph nodes. As the smallest pore on lymphatic vessels is much larger than those in blood capillaries, it is generally belived that only compounds with molecular weight over 16,000 Da rarely gain access to blood capillaries and usually turned to lymphatic capillaries. However, our results proved that Folate-PEG-CKK_2-DTPA with much less molecular weight could be directed to lymph nodes other than blood vessels. Similar results were also found in another previous report, also on Folate-PEG-DTPA-^{99m}Tc agents (27), perhaps related to the linear configuration of PEG.

In the *in vivo* distribution experiment, a significantly higher uptake in popliteal, iliac and inguinal lymph nodes was observed after injection of Folate-PEG-CKK_2-DTPA into footpad, in accordance with another report about lymph nodes mapping in small animal using Evans Blue dye (34). The enhanced uptake in lymphatic nodes may be beneficial for the diagnosis and therapy of the malignancy in lymphatic systems. In addition, this method could potentially provide an alternative for prostate cancer diagnosis and therapy because the iliac also drains the prostate.

SPECT images of Folate-PEG-CKK_2-DTPA in rabbits demonstrated the fast accumulation and clearance of the conjugate in normal lymph nodes, which might be attributed to the amplitude of negative charges considering the affluent terminal carboxy groups in the conjugate (35). The hydrophilic characteristic of PEG section may also play this role, as supposed by a previous study in which PEGylation reduced macrophage uptake of the conjugation (36). The fast clearance nature of the conjugate from normal lymph nodes may reduce the false-positive possibility and thus favors its application in diagnosis of metastatic status. It was not surprising to find the strongest signal in the popliteal lymph nodes, since the popliteal node is the primary draining lymph node following subcutaneous injection in hind feet. The sustained increase of the radio tracer in kidney and bladder indicated a renal elimination pathway for the conjugate and the affluent of folate receptor expressed in kidney proximal tubule as reported (37).

KB cell line was selected for the endocytosis experiment for its high expression of folate receptor. *In vitro* cell endocytosis test demonstrated the uptake of Folate-PEG-CKK_2-DTPA in tumor cells through a folate receptor-mediated mechanism, which was further supported by the *in vivo* and *ex vivo* imaging results. In tumor-bearing mice, significant signal could only be observed from tumor and

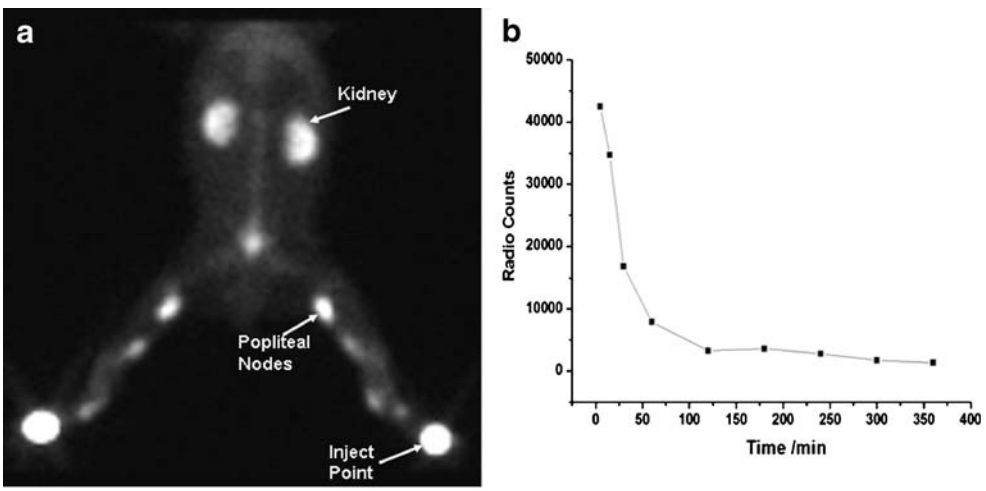

Fig. 5 SPECT imaging of Folate-PEG-CKK_2-DTPA-^{99m}Tc at 3 h in a rabbit after web space injection between digiti pedis in both hind limbs (**a**) and Radio Counts *vs*. Time profiles of left popliteal lymph node over 6 h (**b**).

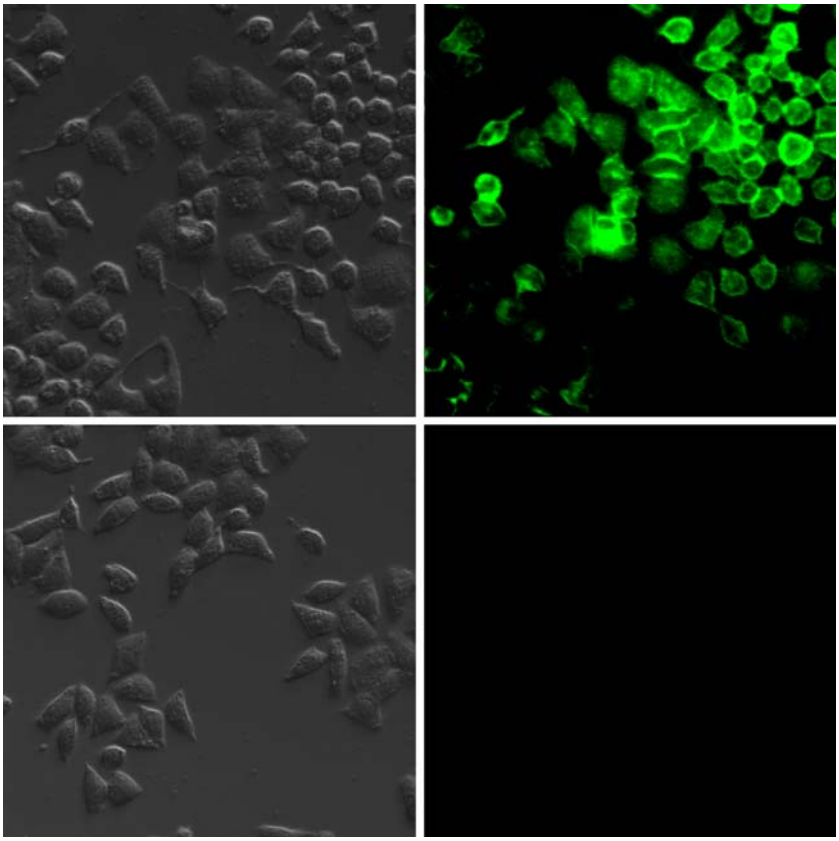

Fig. 6 Fluorescent microscopy of FITC-labeled Folate-PEG-CKK_2-DTPA in KB cells; upper panels show cells incubated with 0.1 μM substrates for 4 h at 37°C; lower panels show cells treated with 0.1 μM substrates containing 1 mM of free folic acid; micrographs were taken in the phase-contrast mode (*left*) and the same field viewed in the fluorescence mode (*right*).

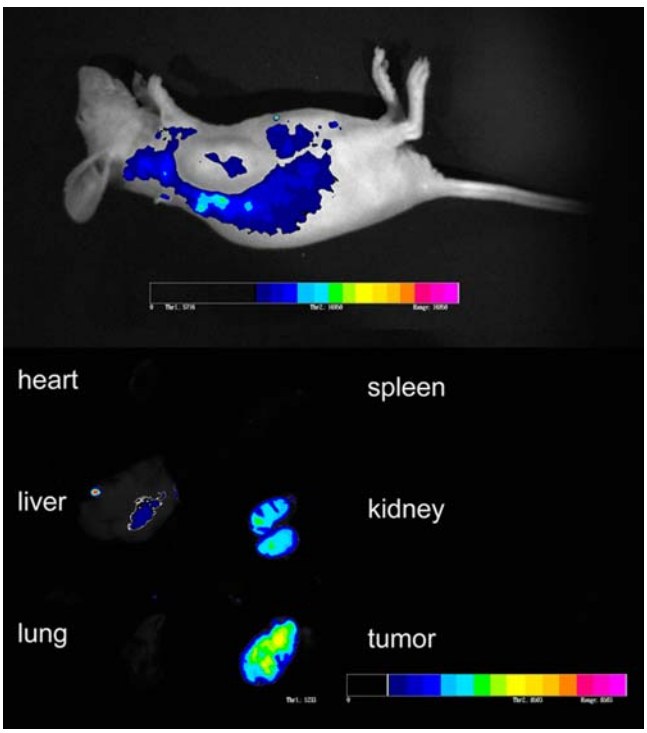

Fig. 7 *In vivo and ex vivo* fluorescent imaging in KB tumor-bearing mouse 2 h after i.v. injection of 1 mg/100 μL Folate-PEG-CKK_2-DTPA labeled with FITC.

kidney. Both the folate receptor-mediated targeting and EPR effects could contribute to the distribution of the molecular in-tumor tissues. The kidney accumulation of the conjugate agreed well with SPECT images.

To prove the potential ability of the conjugation for lymph-metastasized tumor diagnosis, our following study would be focused on sentinel lymph nodes targeting on animal tumor models with lymphatic metastases.

CONCLUSIONS

In summary, Folate-PEG-CKK_2-DTPA showed a fast drainage into the lymphatic system with a subsequent fast clearance. In combination with its capability of being taken up by tumor cells and tissues, the conjugate could be potentially used as a carrier for lymphatic metastasized tumor imaging diagnosis and targeting therapy.

ACKNOWLEDGEMENTS

This work was supported by National Science and Technology Major Project of China (2009ZX09310-006), National Basic Research Program of China (973 Program, 2010CB934000) and National High-Tech Research & Development Program of China (863 program, 2006AA03Z325).

REFERENCES

1. Swartz MA. The physiology of the lymphatic system. Adv Drug Deliv Rev. 2001;50:3–20.
2. Hanahanand D, Weinberg RA. The hallmarks of cancer. Cell. 2000;100:57–70.
3. Oussorenand C, Storm G. Liposomes to target the lymphatics by subcutaneous administration. Adv Drug Deliv Rev. 2001;50:143–56.
4. Torchilin VP. PEG-based micelles as carriers of contrast agents for different imaging modalities. Adv Drug Deliv Rev. 2002;54:235–52.
5. Torabi M, Aquino SL, Harisinghani MG. Current Concepts in Lymph Node Imaging. J Nucl Med. 2004;45:1509–18.
6. Kishimoto H, Kojima T, Watanabe Y, Kagawa S, Fujiwara T, Uno F, *et al. In vivo* imaging of lymph node metastasis with telomerase-specific replication-selective adenovirus. Nat Med. 2006;12:1213–9.
7. Koyama Y, Talanov VS, Bernardo M, Hama Y, Regino CA, Brechbiel MW, *et al.* A dendrimer-based nanosized contrast agent dual-labeled for magnetic resonance and optical fluorescence imaging to localize the sentinel lymph node in mice. J Magn Reson Imaging. 2007;25:866–71.
8. Moghimiand SM, Bonnemain B. Subcutaneous and intravenous delivery of diagnostic agents to the lymphatic system: applications in lymphoscintigraphy and indirect lymphography. Adv Drug Deliv Rev. 1999;37:295–312.
9. Tanis PJ, Boom RPA, Koops HS, Faneyte IF, Peterse JL, Nieweg OE, *et al.* Frozen section investigation of the sentinel node in malignant melanoma and breast cancer. Ann Surg Oncol. 2001;8:222–6.
10. Korst RJ, Ailawadi M, Lee JM, Lee S, Yamada R, Mahtabifard A, *et al.* Adenovirus gene transfer vectors inhibit growth of lymphatic tumor metastases independent of a therapeutic transgene. Hum Gene Ther. 2001;12:1639–49.
11. Konno H, Tadakuma T, Kumai K, Takahashi T, Ishibiki K, Abe O, *et al.* The antitumor effects of adriamycin entrapped in liposomes on lymph node metastases. Jpn J Surg. 1990;20:424–8.
12. Khato J, Priester ER, Sieber SM. Enhanced lymph node uptake of melphalan following liposomal entrapment and effects on lymph node metastasis in rats. Cancer Treat Rep. 1982;66:517–27.
13. Kaledin VI, Matienko NA, Nikolin VP, Gruntenko YV, Budker VG. Intralymphatic administration of liposome-encapsulated drugs to mice: possibility for suppression of the growth of tumor metastases in the lymph nodes. J Natl Cancer Inst. 1981;66:881–7.
14. Cai S, Xie Y, Bagby TR, Cohen MS, Forrest ML. Intralymphatic chemotherapy using a hyaluronan-cisplatin conjugate. J Surg Res. 2008;147:247–52.
15. Oussoren C, Eling WMC, Crommelin DJA, Storm G, Zuidema J. The influence of the route of administration and liposome composition on the potential of liposomes to protect tissue against local toxicity of two antitumor drugs. Biochim Biophys Acta, Biomembranes. 1998;1369:159–72.
16. Sudimackand J, Lee RJ. Targeted drug delivery via the folate receptor. Adv Drug Deliv Rev. 2000;41:147–62.
17. Shia J, Klimstra DS, Nitzkorski JR, Low PS, Gonen M, Landmann R, *et al.* Immunohistochemical expression of folate receptor [alpha] in colorectal carcinoma: patterns and biological significance. Human Pathol. 2008;39:498–505.
18. Nabil FS, Xu W, Susan M, Mourad T, Kwangjae C, Shuming N, *et al.* Examining expression of folate receptor in squamous cell carcinoma of the head and neck as a target for a novel nanotherapeutic drug. Head & Neck. 2009;31:475–81.
19. Kennedy MD, Jallad KN, Thompson DH, Ben-Amotz D, Low PS. Optical imaging of metastatic tumors using a folate-targeted fluorescent probe. J Biomed Opt. 2003;8:636–41.
20. Mathias CJ, Wang S, Waters DJ, Turek JJ, Low PS, Green MA. Indium-111-DTPA-Folate as a potential folate receptor-targeted radiopharmaceutical. J Nucl Med. 1998;39:1579–85.
21. Fisher RE, Siegel BA, Edell SL, Oyesiku NM, Morgenstern DE, Messmann RA, *et al.* Exploratory study of 99mTc-EC20 imaging for identifying patients with folate receptor-positive solid tumors. *J Nucl Med.* jnumed.107.049478 (2008).
22. Muller C, Forrer F, Schibli R, Krenning EP, de Jong M. SPECT study of folate receptor-positive malignant and normal tissues in mice using a novel 99mTc-Radiofolate. J Nucl Med. 2008;49:310–7.
23. Moghimiand M, Moein Moghimi S. Lymphatic targeting of immuno-PEG-liposomes: evaluation of antibody-coupling procedures on lymph node macrophage uptake. J Drug Target. 2008;16:586–90.
24. Moghimi SM. The effect of methoxy-PEG chain length and molecular architecture on lymph node targeting of immuno-PEG liposomes. Biomaterials. 2006;27:136–44.
25. Liu S. Bifunctional coupling agents for radiolabeling of biomolecules and target-specific delivery of metallic radionuclides. Adv Drug Deliv Rev. 2008;60:1347–70.
26. Kaiser RLCE, Bossinger CD, Cook PI. Color test for detection of free terminal amino groups in the solid-phase synthesis of peptides. 1970;34:595–598.
27. Liu M, Xu W, Xu L-J, Zhong G-R, Chen S-L, Lu W-Y. Synthesis and biological evaluation of diethylenetriamine pentaacetic acid-polyethylene glycol-folate: a new folate-derived, (99m)Tc-based radiopharmaceutical. Bioconjug Chem. 2005;16:1126–32.
28. Mathias CJ, Hubers D, Low PS, Green MA. Synthesis of [(99m)Tc]DTPA-folate and its evaluation as a folate-receptor-targeted radiopharmaceutical. Bioconjug Chem. 2000;11:253–7.
29. Bettio A, Honer M, Muller C, Bruhlmeier M, Muller U, Schibli R, *et al.* Synthesis and preclinical evaluation of a folic acid derivative labeled with 18F for PET imaging of folate receptor-positive tumors. J Nucl Med. 2006;47:1153–60.
30. Muller C, Hohn A, Schubiger PA, Schibli R. Preclinical evaluation of novel organometallic 99mTc-folate and 99mTc-pteroate radiotracers for folate receptor-positive tumour targeting. Eur J Nucl Med Mol Imaging. 2006;33:1007–16.
31. Leamon CP, DePrince RB, Hendren RW. Folate-mediated drug delivery: effect of alternative conjugation chemistry. J Drug Target. 1999;7:157–69.
32. Maisano F, Gozzini L, De Haen C. Coupling of DTPA to proteins: a critical analysis of the cyclic dianhydride method in the case of insulin modification. Bioconjug Chem. 2002;3:212–7.
33. McLennan DN, Porter CJH, Charman SA. Subcutaneous drug delivery and the role of the lymphatics. Drug Discov Today Technol. 2005;2:89–96.
34. Harrell MI, Iritani BM, Ruddell A. Lymph node mapping in the mouse. J Immunol Methods. 2008;332:170–4.
35. Hawley AE, Davis SS, Illum L. Targeting of colloids to lymph nodes: influence of lymphatic physiology and colloidal characteristics. Adv Drug Deliv Rev. 1995;17:129–48.
36. Illum L, Hunneyball IM, Davis SS. The effect of hydrophilic coatings on the uptake of colloidal particles by the liver and by peritoneal-macrophages. Int J Pharm. 1986;29:53–65.
37. Birn H, Nielsen S, Christensen EI. Internalization and apical-to-basolateral transport of folate in rat kidney proximal tubule. Am J Physiol Renal Physiol. 1997;272:F70–8.